CONDENSED MATTER PHYSICS

Strain-driven autonomous control of cation distribution for artificial ferroelectrics

Changhee Sohn[1†], Xiang Gao[1], Rama K. Vasudevan[2], Sabine M. Neumayer[2], Nina Balke[2], Jong Mok Ok[1], Dongkyu Lee[1], Elizabeth Skoropata[1], Hu Young Jeong[3], Young-Min Kim[4,5], Ho Nyung Lee[1]*

In past few decades, there have been substantial advances in theoretical material design and experimental synthesis, which play a key role in the steep ascent of developing functional materials with unprecedented properties useful for next-generation technologies. However, the ultimate goal of synthesis science, i.e., how to locate atoms in a specific position of matter, has not been achieved. Here, we demonstrate a unique way to inject elements in a specific crystallographic position in a composite material by strain engineering. While the use of strain so far has been limited for only mechanical deformation of structures or creation of elemental defects, we show another powerful way of using strain to autonomously control the atomic position for the synthesis of new materials and structures. We believe that our synthesis methodology can be applied to wide ranges of systems, thereby providing a new route to functional materials.

INTRODUCTION

On the basis of advances in thin-film synthesis, epitaxial strain, which originates from the lattice mismatch between a film and a substrate, has played a central role in manipulating important physical properties of materials (*1*–*7*) and even revolutionized industries by enabling the development of fast central computing processors (*8*). Ferroelectricity in strained, ultrathin HfO_2 and its potential for ultrahigh density memory (*9*) is another recent example showing the importance of strain engineering in future technologies. While strain has been a control parameter used mainly in condensed matter physics and materials sciences for emergent phenomena and enhanced functionalities, the main roles of strain have been limited to either mechanical deformation of materials or creation of elemental defects. Recently, a theoretical prediction proposed an unreported role of strain in developing new materials by inserting and repositioning individual atoms within a unit cell of materials in a site-specific manner (*10*).

This strain-driven synthesis methodology is illustrated in Fig. 1 with a combination of the layered perovskite $Bi_4Ti_3O_{12}$ (BiT) and simple perovskite ABO_3. BiT is a unique layered ferroelectric material with three oxygen octahedral sublayers sandwiched between two BiO_2^- layers. Its *c* axis is about eight times longer than a simple perovskite (a = 5.448 Å, b = 5.410 Å, and c = 32.840 Å), providing a condition for substitution or addition of ABO_3. The main polarization of this material lies along the [100] direction in the orthorhombic notation. The most attractive properties of this BiT include the robust ferroelectricity against defects and alloying (*11*, *12*) and the layered crystal structure that allows the insertion of $A^{3+}B^{3+}O_3$ perovskites to create multifunctional heterostructures (*12*, *13*). For an example of the latter, if we insert a $BiFeO_3$ (BFO) perovskite into the layered BiT, then it will result in the composite $Bi_5Ti_3FeO_{12}$ (BiTF) with four oxygen octahedral layers between the two BiO_2^- layers as shown in Fig. 1. Note that the inserted Fe ions have degrees of freedom in their positioning; they can be either at two outer octahedral layers or at two inner octahedral layers, two distinct crystallographic positions. The key for this synthesis approach is that the position of inserted Fe ions can be controlled at the subunit cell level by strain as a recent theoretical study predicted (*10*). When Fe ions are located at the outer perovskite layer, its large local tetragonality increases the lattice constant along the *c* axis. As a result, Fe ions prefer to locate at the two outer (inner) octahedral layers in compressively (tensile) strained films with a larger (smaller) *c* lattice constant than that of bulk. However, the predicted control of cationic distribution using strain has yet to be experimentally confirmed.

RESULTS

Synthesis of composite BiTF films using a two-target growth method

We used pulsed laser deposition with two targets, BiT and BFO, to demonstrate the growth control of composite materials by deliberately alloying BFO with the layered perovskite BiT. We accurately calibrated the growth rate per laser pulse and the alternatively ablated each material at subunit cell level on $SrTiO_3$ (STO) substrates to precisely control the composition as we previously demonstrated elsewhere (*12*). Figure 2A shows the evolution of the crystallographic structure seen from x-ray diffraction (XRD) θ-2θ scans as we increase the fraction of BFO. The bottom line shows an XRD scan of a pure BiT film, which is consistent with the BiT structure with the characteristic three octahedral sublayers. As we increased the fraction of BFO in films, the original 004 peak was continuously separated into two, indicating that the stoichiometric BiTF structure with four octahedral layers was created. We note that, while the combination of BiT and $LaCoO_3$ we studied before allowed $LaCoO_3$ to site-specifically "substitute" one of the three Bi-Ti-O perovskite blocks (*12*), the current work "inserted" the BFO perovskite block

[1]Materials Science and Technology Division, Oak Ridge National Laboratory, Oak Ridge, TN 37831, USA. [2]Center for Nanophase Materials Sciences, Oak Ridge National Laboratory, Oak Ridge, TN 37831, USA. [3]UNIST Central Research Facilities, Ulsan National Institute of Science and Technology (UNIST), Ulsan 44919, Republic of Korea. [4]Department of Energy Science, Sungkyunkwan University, Suwon 16419, Republic of Korea. [5]Center for Integrated Nanostructure Physics, Institute for Basic Science, Suwon 16419, Republic of Korea.
*Corresponding author. Email: hnlee@ornl.gov
†Present address: Department of Physics, Ulsan National Institute of Science and Technology (UNIST), Ulsan 44919, Republic of Korea.

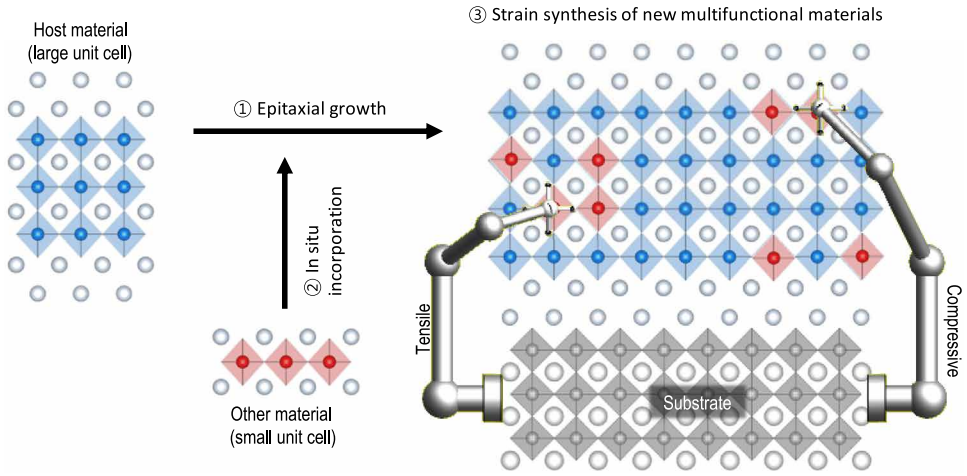

Fig. 1. A schematic diagram of the developed strain synthesis of composite oxide heterostructures. During the epitaxial growth of host materials (BiT) with a large *c* lattice constant, another material (BFO) with a smaller unit cell is incorporated in situ, resulting in a BiTF composite system. There are four octahedral layers with Ti (blue) and Fe (red) ions between two BiO_2^- layers. In bulk, there is no way to control the local distribution of Ti and Fe ions among four octahedral layers. However, strain in thin film can work as nanorobot arms in that Fe ions preferentially locate at inner (outer) octahedral layers under tensile (compressive) strain to reduce the total energy of the system.

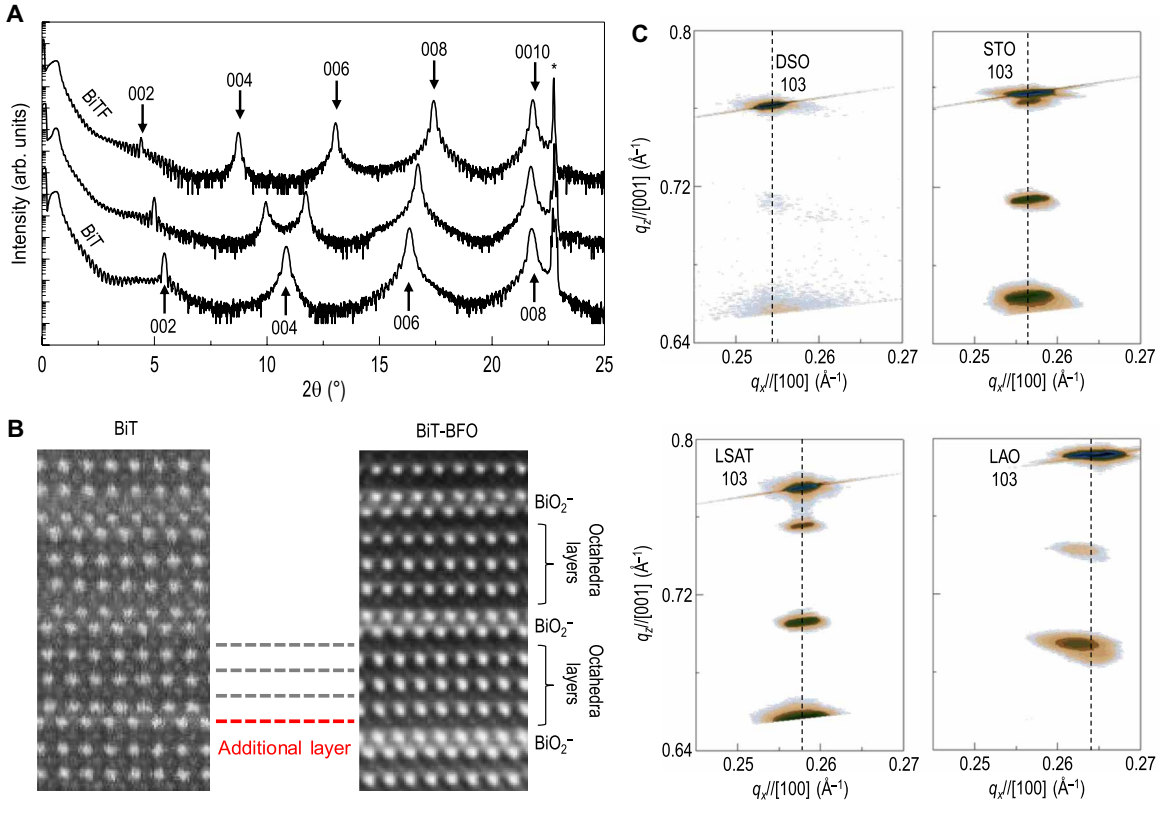

Fig. 2. Structural characterization of BiTF thin films grown on various substrates. (**A**) X-ray diffraction θ-2θ scans of BiTF composite films with the different fraction of BFO blocks. The θ-2θ scans show the structural evolution from BiT with three octahedral layers to BiTF with four octahedral layers as BFO blocks are inserted. The asterisk indicates the 001 peak from the STO substrate. arb. units, arbitrary units. (**B**) HAADF images of BiT (left) and BiTF (right) composite films. While gray dashed lines are three octahedral layers already existing in the BiT film, the red dashed line shows an additional octahedral layer in the BiTF film. It indicates complete insertion of a BFO perovskite block into BiT structures. (**C**) Reciprocal space maps of strained BiTF films grown on four different substrates. Black dashed lines highlight the substrate (103) q_x.

into BiT and increased the number of perovskite blocks in between the two BiO_2^- sublayers. Although we still have to understand the underlying mechanism that determines the substitution or insertion, the first demonstration of positioning an entire perovskite block during the deposition of layered BiT shown here implies that similar methodologies can be used to develop completely new oxide materials and structures in combination of layered and simple oxide perovskites.

Scanning transmission electron microscopy (STEM) further visualizes complete insertion of the additional octahedral layer between adjunct BiO_2^- layers. Figure 2B (left and right) is high-angle annular dark-field (HAADF) images of BiT and BiTF films grown on STO substrates, respectively. The bright, intense signal comes from heavy Bi ions, while weaker signal comes from lighter Ti/Fe ions. As shown in Fig. 2B (left), three octahedral layers marked with gray dashed lines are clearly exhibited between two BiO_2^- layers. For the case of the film grown with incorporation of BFO, on the other hand, additional octahedral layers (red dashed line) were observed, confirming the complete insertion of BFO perovskite blocks into the host BiT. These additional octahedral layers were found uniformly in the wide region of the film (fig. S1).

We further found that this two-target method can be used to synthesize epitaxial BiTF thin films on various substrates with different directions and magnitudes of strain. BiTF is orthorhombic with lattice constant of a_o = 5.4677 Å, b_o = 5.4396 Å, and c_o = 41.2475 Å (*14*), which can be represented as pseudo-tetragonal lattice constant of a_t = 3.8563 Å. In addition to the STO substrate, which induces 1.3% tensile strain in BiT, we used $LaAlO_3$ (LAO), $[(LAO)_{0.3}$-$(SrAl_{0.5}Ta_{0.5}O_3)_{0.7}]$ (LSAT), and $DyScO_3$ (DSO) substrates to change the strain state from −1.8% (compressive) on LAO to 2.2% (tensile) on DSO. While the thickness of BiTF films on LAO, LSAT, and STO substrates is about 40 nm, we grew BiTF on DSO, which has the largest lattice mismatch, only about 10 nm in thickness. Because of the large lattice mismatch between BiTF and DSO, we found that the strain of BiTF film was immediately relaxed when the film thickness exceeded 10 nm. Figure 2C exhibits reciprocal space maps near the 103 peak of the substrates. While BiTF films remain fully strained on STO and LSAT substrates with a moderate lattice mismatch, BiTF films on DSO and LAO substrates are partially relaxed because of large lattice mismatch. However, by comparing with the bulk lattice constants, we found that those films on DSO and LAO substrate still have 1.8 and −0.9% strain remaining, respectively.

Experimental observation of local Fe ion distributions in strained BiTF films

To visualize the strain-dependent distribution of Fe ions at the atomic scale, we conducted energy-dispersive x-ray (EDX) spectroscopy mapping combined with STEM on BiTF films. Figure 3 shows schematic crystal structures, HAADF images, and EDX mapping images/profiles on each element edge (Bi, Ti, Fe, and O) of films grown on LAO, STO, and DSO substrates. We excluded the data of BiTF film on LSAT because the site preference of Fe ions appeared to be intermediate between the films on LAO and STO (fig. S2). All STEM images were taken along the [100] direction in the pseudo-tetragonal notation (equivalent to the [110] direction in the orthorhombic notation). In the HAADF images, the bright contrasts originate from the heavy Bi, while the less bright contrasts are from light Ti/Fe ions.

Atomically resolved EDX mapping and its profile revealed the distinct evolution in preferential positions of Fe ions among four octahedral layers with strain. In the profile of Fe *K* edge (the rightmost column of Fig. 3), the position of four octahedral layers was denoted by numbers. For the case of the film grown on LAO with −0.9% compressive strain, the Fe *K* edge signal is enhanced in outer octahedral layers (#1 and #4 layers). When we change the strain to 1.3% tensile strain using an STO substrate, the site preference of Fe ions almost disappears, and they are rather randomly distributed among octahedral layers. If we further increase the tensile strain to 1.8% with a DSO substrate, then the site preference of Fe ions becomes opposite to the case of LAO, and they prefer to locate at the inner octahedral layers (#2 and #3 layers). The EDX elemental mapping confirms that the practical size of strain on BiTF films controls the local distribution of Fe ions within the unit cell as schematically shown in Fig. 1. The observed trend is consistent with a recent theoretical calculation that tensile (compressive) strain stabilizes the inner (outer) configuration of Fe ions. (*10*) Therefore, although strain is not the only variable in four substrates, the excellent agreement with the theoretical prediction supports that strain plays a main role in controlling Fe ion distribution.

In addition to aforementioned intrinsic phenomena by strain, we would like to discuss some extrinsic effects on cationic distribution we have observed in the films. Unlike other films, BiTF films on DSO substrates showed a finite EDX signal of Fe ions in BiO_2^- layers (Fig. 3C). It might originate from intermixing of cations due to a large lattice mismatch between BiTF film and DSO substrate. For all films, we observed a slightly higher intensity of Fe EDX signals in #1 layers (close to the surface) than #4 layers (close to the substrate). This effect becomes significant in the BiTF film on STO (Fig. 3B) where the intrinsic preference of cation distribution is almost vanished. Because these two outer layers are identical in the crystallographic point of view, it should be an extrinsic effect. Although the exact origin of these phenomena is not clear, we speculate that it might be related to a detailed growth mechanism. In the process of thin-film growth, inversion symmetry always remains broken, so do nucleation of materials and migration of cations. This effect can be considerable when there is little preference in position of cations. Although this effect was not deliberated, it could affect out-of-plane ferroelectricity as discussed below.

Evolution of physical properties in BiT films with incorporation of BFO blocks

A logical question here is how inserting and positioning Fe ions within BiT can affect the macroscopic properties. We first focused on the optical properties, which are important not only for fundamental understandings on electronic structures, but also for technological applications. Figure 4 (A to D) shows the real part of optical conductivity $\sigma_1(\omega)$ of BiT (black lines) and BiTF (red lines) films grown on each substrate. We note that inserting BFO blocks reduces the bandgap of the original BiT films by ~0.5 eV. It demonstrates the capability of our synthesis approach for bandgap tuning, important for photovoltaic applications as reported in a previous study with a BiT and $LaCoO_3$ composite system (*12*). Because Fe^{3+} (d^5) and Ti^{4+} (d^0) ions do not have low-energy d-d excitations, the lowest optical transition of BiTF films should be charge transfer transitions from O 2p to Fe/Ti 3d orbitals. Therefore, we attribute the observed reduction in the bandgap to the fact that charge transfer energy of Fe^{3+} octahedra is smaller than that of Ti^{4+} octahedra, consistent with previous density functional theory (DFT) calculations (*15*). The bandgap reduction observed here, however, is mostly due to the

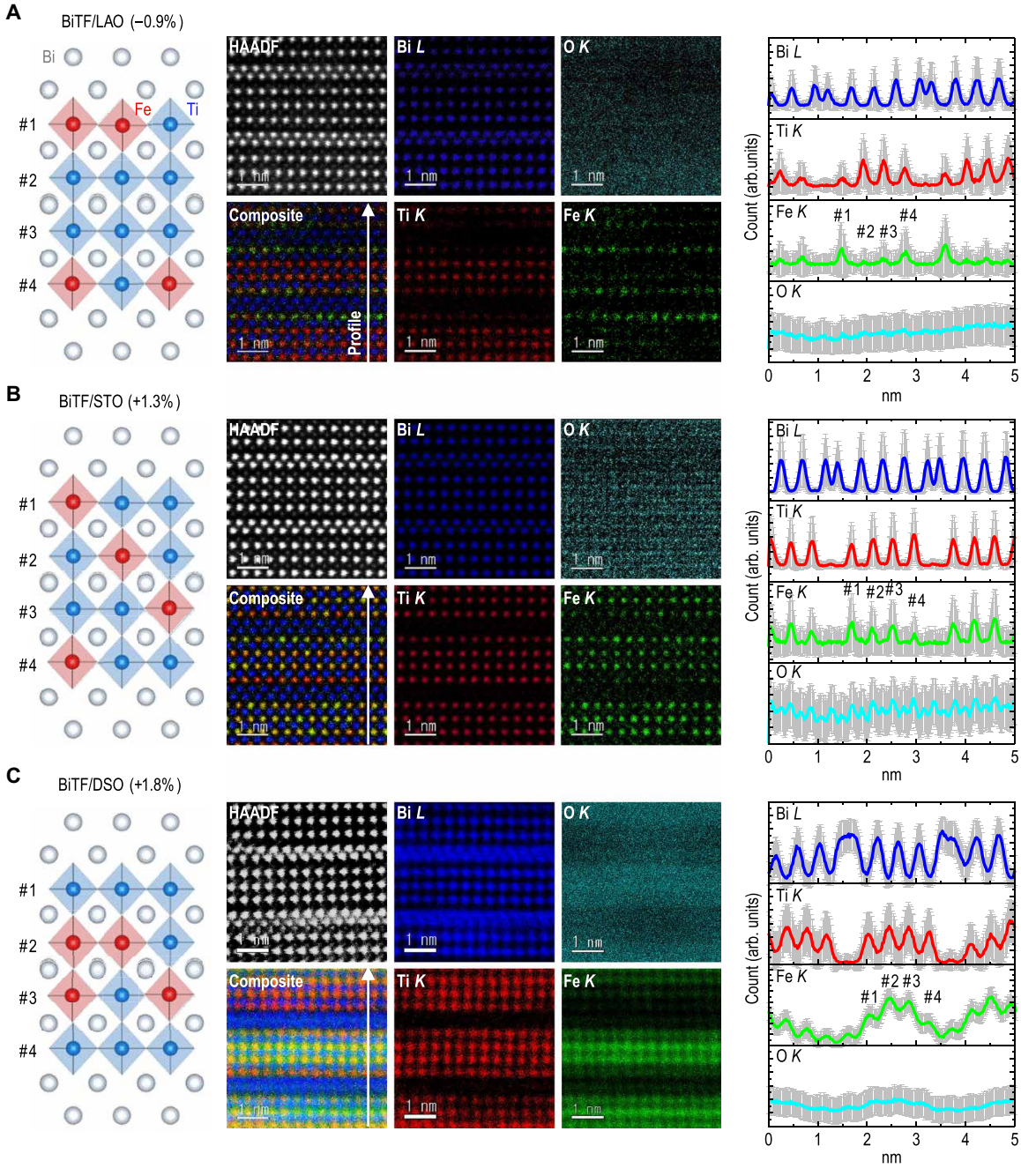

Fig. 3. Strain-dependent Fe distribution in BiTF films. Atomically resolved STEM-EDX mapping of BiTF grown on (**A**) LAO (−0.9%), (**B**) STO (1.3%), and (**C**) DSO (1.8%) substrates. The leftmost column exhibits schematic diagrams of local Fe distribution in BiTF. The middle column exhibits HAADF, element-selective EDX, and overlaid EDX images. The Fe *K*-edge mapping shows that Fe ions are preferentially located at outer (inner) octahedral layer in BiTF/LAO (DSO) and randomly distributed in BiTF/STO. The rightmost column is line profiles of each element along the white arrows in EDX maps.

insertion of BFO blocks, and there is no qualitative difference between the cases of Fe ions in inner and outer octahedral layers.

More interesting subject would be the relationship between ferroelectricity of BiTF films and cationic distribution of Fe ions. Because BiTF films are expected to show ferroelectric polarization along the in-plane [100] (orthorhombic notation) direction, typical capacitor geometry for ferroelectric measurement is hardly conducted. Instead, we used contact Kelvin probe force microscopy (cKPFM) (*16*, *17*), an advanced piezoresponse force microscopy (PFM) technique, to examine piezoelectric properties along the lateral [100] direction in the orthorhombic notation and the vertical [001] direction of the films. Note that, while hysteresis response in conventional PFM cannot guarantee ferroelectricity because of nonferroelectric electromechanical effect, cKPFM gives insight into voltage-dependent processes

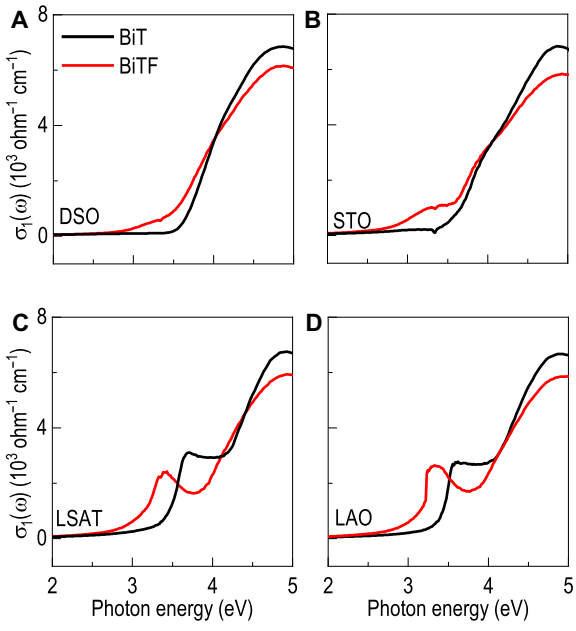

Fig. 4. Bandgap reduction and unexpected out-of-plane ferroelectric polarization in BiTF films. (**A** to **D**) $\sigma_1(\omega)$ of BiT (black) and BiTF (red) films on each substrate. The observed reduction of the bandgap by inserting BFO blocks implies that charge transfer energy between Fe 3d and O 2p orbitals is smaller than that between Ti 3d and O 2p orbitals.

responsible for the hysteresis behavior as a way to rule out these effects (*18*).

Strong substrate dependence on lateral and vertical ferroelectricity was observed. Figure 5 (A to D) shows lateral cKPFM measurements of the film on each substrate. We observed a clear nonlinear, hysteresis signal in BiTF films on LSAT and STO substrates, while those on LAO and DSO substrates showed weak and negligible ferroelectric behaviors, respectively. The observed strain dependence was inconsistent with the previous DFT calculation, where ferroelectric polarization varies by only about 10% in the range of strain we used (from −0.9 to 1.8%). Another unusual observation in their ferroelectricity is the finite ferroelectric behaviors along the vertical direction in the BiTF film on STO substrate. Figure 5 (E to H) shows vertical cKPFM results from the film on each substrate. For the films grown on DSO, LSAT, and LAO, there is no hysteresis behavior, indicating the absence of ferroelectric polarization along the [001] direction. It is consistent with the known fact that there is no ferroelectric polarization in BiTF along the [001] direction (*19*), because of the mirror symmetry in even-layer Aurivillius structure. However, as shown in Fig. 5G, clear hysteresis behaviors have found in the BiTF film grown on STO.

DISCUSSION

Although the origin of the observed substrate-dependent ferroelectricity is not clear, we doubt that a simple structural change by strain can explain our observation. It is because (i) the structural change by lattice and/or symmetry mismatch should be captured by the previous DFT calculations (*10*), where the ferroelectric polarization changed by only about 10% within our strain range, (ii) the ferroelectricity in Aurivillius materials such as Bi_2WO_6 did not reveal strong substrate dependence (*20*), and (iii) the trend of ferroelectric polarization is nonmonatomic with strain change. Rather, because BiTF films on LAO and DSO substrates have preferential positions of Fe ions, suppression of the lateral ferroelectric polarization could be related to cation ordering.

Below is one of the plausible explanations how cation order/disorder can affect ferroelectricity in BiTF, based on different amplitudes of rotation/tilt modes for different cations. It has been previously reported in $PbTiO_3$/STO superlattices, for example, that improper hybrid ferroelectricity emerges from the different tilting amplitudes of octahedra in alternating Pb and Sr layers (*21*, *22*). Similarly, the net polarization in BiTF along the [100] direction is mainly attributed to the displacement of Bi ions of perovskite blocks with cooperative octahedral tilt/rotation (*23*–*25*). For the case of perfect cation ordering, the BiTF contains two Ti and two $Fe_{0.5}/Ti_{0.5}$ octahedral layers, implying strong inhomogeneity along the *c* axis. Because of different tilting/rotation amplitudes between Fe and Ti octahedra, this inhomogeneity among layers can disturb coherent polar tilt/rotation modes, thereby reducing the ferroelectric polarization.

The vertical polarization found in the BiTF/STO film, on the other hand, can be related to extrinsic mirror symmetry breaking by cationic distribution. Because of the symmetry in even layer Aurivillius phases, the vertical ferroelectric polarization must be cancelled out. Therefore, the only way to have finite out-of-plane polarization is breaking that symmetry. As mentioned above, there is extrinsic preference of Fe ion position between #1 and #4 layers (Fig. 3), which is particularly strong in the BiTF film on STO. Therefore, out-of-plane ferroelectric polarization could not be cancelled out, resulting in a finite cKPFM signal along the [001] direction.

So far, we have demonstrated the unique strain-driven synthesis paradigm (Fig. 1), which enables us not only to insert atoms, but also to autonomously direct them to a specific crystallographic position of matter. It should be noted that our method developed here is distinct from well-known synthesis methodologies, such as conventional heterostructure engineering or simple alloying of two materials. In the history of modern science, advances in synthesis have opened a new field of research and provided platforms underpinning future technologies as evidenced by representative examples such as semiconductor p-n junctions (*26*–*28*), conducting polymers (*29*, *30*), graphene (*31*–*33*), and other novel heterostructures (*34*–*37*). Therefore, we expect that the strain-driven autonomous control of atomic positions may boost research in materials sciences and condensed matter physics to develop novel multifunctional composite systems.

One might consider that, because BiTF exists stable in nature, inserting BFO blocks using the two-target method here is redundant. However, there are at least two advantages in our method compared to conventional solid-state reaction in addition to controllability of cationic positions. First, incorporation of additional blocks (BFO for our case) occurs during the deposition, allowing us to change mixing ratio of two materials easily. Second, we believe such a non-equilibrium method can be applied to a wide range of metastable materials to synthesize otherwise unstable composite systems. For example, all ABO_3 perovskites (A = La^{3+} and Bi^{3+} and B = transition metal ions) can be inserted and controlled in host ferroelectric BiT. Instead of Aurivillius phases, other extended lattice materials, e.g., Ruddlesden-Popper phases, are also viable examples for host materials. Both dynamic deposition process and strain from substrate are expected to incorporate two materials into a new system, which do not exist naturally. Thus, similar synthesis approaches with numerous combinations of materials are highly encouraged.

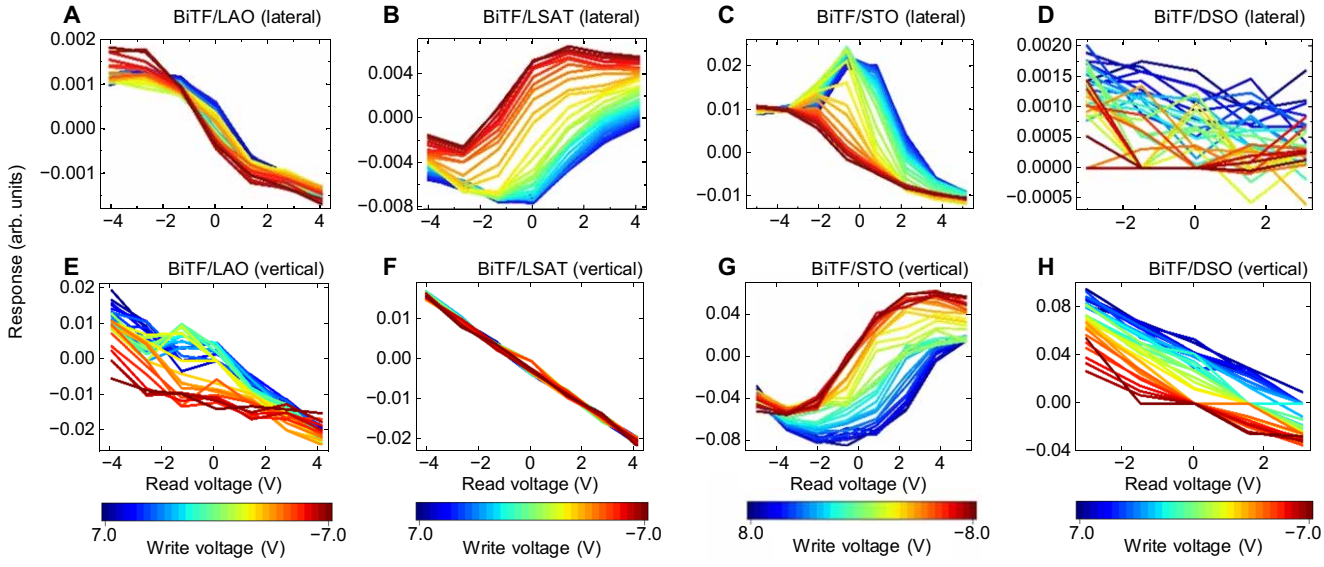

Fig. 5. Strain-dependent in-plane and out-of-plane ferroelectric polarizations in BiTF films. (**A** to **D**) Lateral cKPFM measured along the orthorhombic [100] direction after application of different voltage pulses, as a function of read voltage. Clear hysteresis behaviors are observed in the films on LSAT and STO substrates, while ferroelectricity is unclear and strongly suppressed in the films on LAO and DSO. This result implies that the randomness of Fe ion position plays a role in stabilizing the ferroelectricity. (**E** to **H**) Vertical cKPFM curves of BiTF films on each substrate. Only the film on STO shows clear out-of-plane ferroelectric hysteresis behaviors, which are forbidden by symmetry in bulk. We attribute this unexpected polarization to extrinsic asymmetry of cationic distribution signified with intrinsic random preference by moderate tensile strain.

We would like to additionally address the limitations of current work and suggest possible future research. Using cKPFM, we provided experimental evidence that the ferroelectric properties might depend on the cationic distribution. However, a thorough understanding of these phenomena is far from complete, and our explanation about different amplitudes of tilting/rotation of octahedra remains speculative. Further investigation into this problem is needed from both experimental and theoretical perspective. Thus, it would be very interesting if magnetic materials can be incorporated with the same method. It could be a promising way to synthesize multiferroic materials and to control its magnetic ground state via cationic distribution. Note that, depending on specific distribution of magnetic ions, their percolation behaviors can be significantly affected.

MATERIALS AND METHODS

Synthesis of BiTF composite film

We fabricated (001)-oriented BiTF epitaxial films on four different substrates using pulsed laser deposition with two targets. We alternatively ablated two stoichiometric targets, BiT and BFO. The ratio of number of pulses for BiT and BFO targets was 2:5 in our setup for stoichiometric BiTF films. Note that the number of pulses we used for each period (two pulses for BiT and five pulses for BFO) is much less than the pulses needed for single unit cell of each material, thereby promoting uniform mixing of two materials. The growth temperature, oxygen partial pressure, laser fluence, and repetition rate for all samples were 700°C, 100 mtorr, 1.5 J/cm^2, and 5 Hz, respectively. All films showed high quality, single phase, and perfect epitaxy with substrates, confirmed by a four-circle XRD (PANalytical).

Structure characterization and elemental mapping

The focused ion beam (FIB; FEI Helios Nano Lab 450) slicing and lift-out process was used to make thin cross-sectional samples for atomic-scale STEM and EDX analyses. The samples were further milled by Ar ion beam accelerated at 700 V (Fischione Model 1040 NanoMill) to remove damaged surface layers formed by heavy Ga ion beam milling in the FIB instrument. Atomic structure images of the samples were taken by a 200-kV aberration-corrected STEM (JEM-ARM200CF, JEOL) with a convergence semiangle of ~23 mrad. The acceptance angle of the HAADF detector was 70 to 175 mrad. Atomically resolved elemental maps of the samples were acquired by a dual-type EDX detector (JED-2300T, JEOL) with a large effective solid angle (Ω = ~1.2 sr) and a highly focused electron probe (~1.1 Å) in the same HAADF-STEM imaging mode.

PFM and cKPFM

A commercially available instrument (Asylum Research, Cypher AFM) was used to perform PFM and cKPFM under ambient conditions with a budget sensor cantilever with free resonance nominally 70 kHz with stiffness k ~ 1.0 N/m (nominal). PFM experiments were performed using the band excitation technique (*16*, *17*), and the contact resonance peaks for cantilever deflection and torsion are fitted using a simple harmonic oscillator to extract vertical and lateral PFM amplitude and phase, respectively.

Spectroscopic ellipsometry

An M-2000 ellipsometer (J.A. Woollam Co.) was used to obtain two ellipsometric parameters, ψ and Δ, for a thin film and a bare STO substrate at room temperature. A two-layer model composed of the substrate and the film was constructed to determine the optical constant of the film. The thickness of the film was determined by separate x-ray reflectometry measurement and fixed during the fitting.

SUPPLEMENTARY MATERIALS

Supplementary material for this article is available at http://advances.sciencemag.org/cgi/content/full/7/18/eabd7394/DC1

REFERENCES AND NOTES

1. J. R. Petrie, V. R. Cooper, J. W. Freeland, T. L. Meyer, Z. Zhang, D. A. Lutterman, H. N. Lee, Enhanced bifunctional oxygen catalysis in strained $LaNiO_3$ perovskites. *J. Am. Chem. Soc.* **138**, 2488–2491 (2016).
2. A. Kushima, B. Yildiz, Oxygen ion diffusivity in strained yttria stabilized zirconia: Where is the fastest strain? *J. Mater. Chem.* **20**, 4809–4819 (2010).
3. H. N. Lee, H. M. Christen, M. F. Chisholm, C. M. Rouleau, D. H. Lowndes, Strong polarization enhancement in asymmetric three-component ferroelectric superlattices. *Nature* **433**, 395–399 (2005).
4. J. Haeni, P. Irvin, W. Chang, R. Uecker, P. Reiche, Y. L. Li, S. Choudhury, W. Tian, M. E. Hawley, B. Craigo, A. K. Tagantsev, X. Q. Pan, S. K. Streiffer, L. Q. Chen, S. W. Kirchoefer, J. Levy, D. G. Schlom, Room-temperature ferroelectricity in strained $SrTiO_3$. *Nature* **430**, 758–761 (2004).
5. K. J. Choi, M. Biegalski, Y. L. Li, A. Sharan, J. Schubert, R. Uecker, P. Reiche, Y. B. Chen, X. Q. Pan, V. Gopalan, L.-Q. Chen, D. G. Schlom, C. B. Eom, Enhancement of ferroelectricity in strained $BaTiO_3$ thin films. *Science* **306**, 1005–1009 (2004).
6. J. Wang, J. B. Neaton, H. Zheng, V. Nagarajan, S. B. Ogale, B. Liu, D. Viehland, V. Vaithyanathan, D. G. Schlom, U. V. Waghmare, N. A. Spaldin, K. M. Rabe, M. Wuttig, R. Ramesh, Epitaxial $BiFeO_3$ multiferroic thin film heterostructures. *Science* **299**, 1719–1722 (2003).
7. J.-P. Locquet, J. Perret, J. Fompeyrine, E. Mächler, J. W. Seo, G. Van Tendeloo, Doubling the critical temperature of $La_{1.9}Sr_{0.1}CuO_4$ using epitaxial strain. *Nature* **394**, 453–456 (1998).
8. M. Ieong, B. Doris, J. Kedzierski, K. Rim, M. Yang, Silicon device scaling to the sub-10-nm regime. *Science* **306**, 2057–2060 (2004).
9. T. Shiraishi, K. Katayama, T. Yokouchi, T. Shimizu, T. Oikawa, O. Sakata, H. Uchida, Y. Imai, T. Kiguchi, T. J. Konno, H. Funakubo, Impact of mechanical stress on ferroelectricity in $(Hf_{0.5}Zr_{0.5})O_2$ thin films. *Appl. Phys. Lett.* **108**, 262904 (2016).
10. A. Y. Birenbaum, C. Ederer, Controlling the cation distribution and electric polarization with epitaxial strain in Aurivillius-phase $Bi_5FeTi_3O_{15}$. *Appl. Phys. Lett.* **108**, 082903 (2016).
11. J. F. Scott, *Ferroelectric Memories* (Springer Science & Business Media, 2013), vol. 3.
12. W. S. Choi, M. F. Chisholm, D. J. Singh, T. Choi, G. E. Jellison Jr., H. N. Lee, Wide bandgap tunability in complex transition metal oxides by site-specific substitution. *Nat. Commun.* **3**, 689 (2012).
13. J. Wang, Z. Chen, H. Huang, J. Cui, W. Zhang, Z. Fu, R. Peng, W. Yan, Y. Lu, Realizing semiconductivity by a large bandgap tuning in $Bi_4Ti_3O_{12}$ via inserting $La_{1-x}Sr_xMnO_3$ perovskite layers. *Appl. Phys. Lett.* **110**, 212102 (2017).
14. F. Kubel, H. Schmid, X-ray room temperature structure from single crystal data, powder diffraction measurements and optical studies of the Aurivillius phase $Bi_5(Ti_3Fe)O_{15}$. *Ferroelectrics* **129**, 101–112 (1992).
15. Z. Zhong, P. Hansmann, Band alignment and charge transfer in complex oxide interfaces. *Phys. Rev. X* **7**, 011023 (2017).
16. S. Jesse, S. V. Kalinin, R. Proksch, A. P. Baddorf, B. J. N. Rodriguez, The band excitation method in scanning probe microscopy for rapid mapping of energy dissipation on the nanoscale. *Nanotechnology* **18**, 435503 (2007).
17. S. Jesse, B. Mirman, S. V. Kalinin, Resonance enhancement in piezoresponse force microscopy: Mapping electromechanical activity, contact stiffness, and *Q* factor. *Appl. Phys. Lett.* **89**, 022906 (2006).
18. R. K. Vasudevan, N. Balke, P. Maksymovych, S. Jesse, S. V. Kalinin, Ferroelectric or non-ferroelectric: Why so many materials exhibit "ferroelectricity" on the nanoscale. *Appl. Phys. Rev.* **4**, 021302 (2017).
19. S. Nakashima, H. Fujisawa, S. Ichikawa, J. M. Park, T. Kanashima, M. Okuyama, M. Shimizu, Structural and ferroelectric properties of epitaxial $Bi_5Ti_3FeO_{15}$ and natural-superlattice-structured $Bi_4Ti_3O_{12}$–$Bi_5Ti_3FeO_{15}$ thin films. *J. Appl. Phys.* **108**, 074106 (2010).
20. C. Wang, X. Ke, J. Wang, R. Liang, Z. Luo, Y. Tian, D. Yi, Q. Zhang, J. Wang, X.-F. Han, G. Van Tendeloo, L.-Q. Chen, C.-W. Nan, R. Ramesh, J. Zhang, Ferroelastic switching in a layered-perovskite thin film. *Nat. Commun.* **7**, 10636 (2016).
21. M. Dawber, C. Lichtensteiger, M. Cantoni, M. Veithen, P. Ghosez, K. Johnston, K. M. Rabe, J.-M. Triscone, Unusual behavior of the ferroelectric polarization in $PbTiO_3$/$SrTiO_3$ superlattices. *Phys. Rev. Lett.* **95**, 177601 (2005).
22. E. Bousquet, M. Dawber, N. Stucki, C. Lichtensteiger, P. Hermet, S. Gariglio, J.-M. Triscone, P. Ghosez, Improper ferroelectricity in perovskite oxide artificial superlattices. *Nature* **452**, 732–736 (2008).
23. C. H. Hervoches, A. Snedden, R. Riggs, S. H. Kilcoyne, P. Manuel, P. Lightfoot, Structural behavior of the four-layer Aurivillius-phase ferroelectrics $SrBi_4Ti_4O_{15}$ and $Bi_5Ti_3FeO_{15}$. *J. Solid State Chem.* **164**, 280–291 (2002).
24. A. Y. Birenbaum, C. Ederer, Potentially multiferroic Aurivillius phase $Bi_5FeTi_3O_{15}$: Cation site preference, electric polarization, and magnetic coupling from first principles. *Phys. Rev. B* **90**, 214109 (2014).
25. R. Withers, J. Thompson, A. D. Rae, The crystal chemistry underlying ferroelectricity in $Bi_4Ti_3O_{12}$, Bi_3TiNbO_9, and Bi_2WO_6. *J. Solid State Chem.* **94**, 404–417 (1991).
26. W. Shockley, The theory of p-n junctions in semiconductors and p-n junction transistors. *Bell Labs Tech. J.* **28**, 435–489 (1949).
27. J. Bardeen, W. H. Brattain, The transistor, a semi-conductor triode. *Phys. Rev.* **74**, 230–231 (1948).
28. R. S. Ohl, Light-sensitive electric device, U.S. Patent No. 2,402,662 (1946).
29. H. Shirakawa, E. J. Louis, A. G. MacDiarmid, C. K. Chiang, A. J. Heeger, Synthesis of electrically conducting organic polymers: Halogen derivatives of polyacetylene, $(CH)_x$. *J. Chem. Soc. Chem. Commun.*, 578–580 (1977).
30. C. K. Chiang, C. R. Fincher, Y. W. Park, A. J. Heeger, H. Shirakawa, E. J. Louis, S. C. Gau, A. G. MacDiarmid, Electrical conductivity in doped polyacetylene. *Phys. Rev. Lett.* **39**, 1098–1101 (1977).
31. Y. Zhang, Y.-W. Tan, H. L. Stormer, P. Kim, Experimental observation of the quantum Hall effect and Berry's phase in graphene. *Nature* **438**, 201–204 (2005).
32. K. S. Novoselov, A. K. Geim, S. V. Morozov, D. Jiang, M. I. Katsnelson, I. V. Grigorieva, S. V. Dubonos, A. A. Firsov, Two-dimensional gas of massless Dirac fermions in graphene. *Nature* **438**, 197–200 (2005).
33. K. Novoselov, D. Jiang, F. Schedin, T. J. Booth, V. V. Khotkevich, S. V. Morozov, A. K. Geim, Two-dimensional atomic crystals. *Proc. Natl. Acad. Sci. U.S.A.* **102**, 10451–10453 (2005).
34. J. A. Mundy, C. M. Brooks, M. E. Holtz, J. A. Moyer, H. Das, A. F. Rébola, J. T. Heron, J. D. Clarkson, S. M. Disseler, Z. Liu, A. Farhan, R. Held, R. Hovden, E. Padgett, Q. Mao, H. Paik, R. Misra, L. F. Kourkoutis, E. Arenholz, A. Scholl, J. A. Borchers, W. D. Ratcliff, R. Ramesh, C. J. Fennie, P. Schiffer, D. A. Muller, D. G. Schlom, Atomically engineered ferroic layers yield a room-temperature magnetoelectric multiferroic. *Nature* **537**, 523–527 (2016).
35. J. Chakhalian, J. W. Freeland, H. U. Habermeier, G. Cristiani, G. Khaliullin, M. van Veenendaal, B. Keimer, Orbital reconstruction and covalent bonding at an oxide interface. *Science* **318**, 1114–1117 (2007).
36. C. H. Ahn, J.-M. Triscone, J. Mannhart, Electric field effect in correlated oxide systems. *Nature* **424**, 1015–1018 (2003).
37. A. Ohtomo, D. A. Muller, J. L. Grazul, H. Y. Hwang, Artificial charge-modulationin atomic-scale perovskite titanate superlattices. *Nature* **419**, 378–380 (2002).

Acknowledgments: We thank A. Y. Birenbaum for discussion. **Funding:** This work was supported by the U.S. Department of Energy (DOE), Office of Science, Basic Energy Sciences, Materials Sciences and Engineering Division. A portion of this research was conducted at the Center for Nanophase Materials Sciences (spectroscopic ellipsometry and PFM), which is a U.S. DOE Office of Science User Facility. Y.-M.K. acknowledges the financial support provided by the Institute for Basic Science (IBS-R011-D1) and Creative Materials Discovery Program (NRF-2015M3D1A1070672) through the NRF grant. **Author contributions:** C.S. conducted sample synthesis, XRD, and optical measurements with help from J.M.O., D.L., and E.S. R.K.V., S.M.N., and N.B. worked on PFM measurements and analyses. X.G., H.Y.J., and Y.-M.K. performed STEM measurements. H.N.L. initiated the research and supervised the work. All authors participated in writing the manuscript. **Competing interests:** The authors declare that they have no competing interests. **Data and materials availability:** All data needed to evaluate the conclusions in the paper are present in the paper and/or the Supplementary Materials. Additional data related to this paper may be requested from the authors.

Submitted 10 July 2020
Accepted 10 March 2021
Published 28 April 2021
10.1126/sciadv.abd7394

Citation: C. Sohn, X. Gao, R. K. Vasudevan, S. M. Neumayer, N. Balke, J. M. Ok, D. Lee, E. Skoropata, H. Y. Jeong, Y.-M. Kim, H. N. Lee, Strain-driven autonomous control of cation distribution for artificial ferroelectrics. *Sci. Adv.* **7**, eabd7394 (2021).

ScienceAdvances

Strain-driven autonomous control of cation distribution for artificial ferroelectrics

Changhee SohnXiang GaoRama K. VasudevanSabine M. NeumayerNina BalkeJong Mok OkDongkyu LeeElizabeth SkoropataHu Young JeongYoung-Min KimHo Nyung Lee

Sci. Adv., 7 (18), eabd7394. • DOI: 10.1126/sciadv.abd7394

Science Advances (ISSN 2375-2548) is published by the American Association for the Advancement of Science. 1200 New York Avenue NW, Washington, DC 20005. The title *Science Advances* is a registered trademark of AAAS.